

HYDROLOGICAL BUDGET IN THE TROPICAL PACIFIC

Xiaosu Xie* and W. Timothy Liu
Jet Propulsion Laboratory
California Institute of Technology, Pasadena, CA

ABSTRACT

Applying high resolution space-based measurements from microwave radiometers and scatterometers, surface fresh water flux ($E - P$) and divergence of integrated moisture transport ($\nabla \cdot \Theta$) are derived over the ocean. They reveal major climatological features of the tropical and subtropical oceans. The seasonal and interannual variations of $E - P$ and $\nabla \cdot \Theta$ are examined through empirical orthogonal function analysis. The seasonal cycle is dominated by meridional migration of deep convection in the intertropical convergence zone (ITCZ). A double ITCZ feature exists in both $E - P$ and $\nabla \cdot \Theta$. The leading mode of interannual variability is consistent with El Niño/Southern Oscillation warm events. Eastward shift of the western Pacific deep convection results in lower sea surface salinity in the equatorial central Pacific. In contrast, the south Pacific convergence zone is characterized by stronger evaporation, reduced convection, and saltier water during the warm events.

1. INTRODUCTION

Integration of the equation for conservation of atmospheric water vapor in the vertical gives

$$\frac{\partial W}{\partial t} + \nabla \cdot \Theta = E - P \quad (1)$$

$$\text{where } \Theta = \frac{1}{g} \int_0^P q u dp \quad (2)$$

is the integrated moisture transport and

$$W = \frac{1}{g} \int_0^{P_s} q dp \quad (3)$$

is the precipitable water. In these equations, E is the evaporation, P is the precipitation, g is the acceleration due to gravity, p is the pressure, P_s is the pressure at the surface, q and \mathbf{u} are the specific humidity and wind vector at a certain level. Symbols in bold are vector quantities.

The oceans are the major reservoirs of water. Moisture is brought to the atmosphere by E over ocean, redistributed through Θ , and returns to the oceans and landmasses as P . $E - P$ into the ocean has to be balanced by the change of salinity and salt advection into the surface mixed layer.

In situ observations for both $E - P$ and salinity are sparse and intermittent, which severely limit our understanding of the major components of hydrological cycle. However, space-based observations allow us to estimate $E - P$ and $\nabla \cdot \Theta$ over the oceans at a broad spectrum of time scales, which will be presented in Section 2.

* Corresponding author address: Xiaosu Xie, M/S 300-323, 4800 Oak Grove Dr., Jet Propulsion Laboratory, Pasadena, CA 91109; Email: xiaosu@pacific.jpl.nasa.gov.

In spite of the observational limitation, Delcroix and Henin (1991) attempted to quantify the role of surface hydrologic forcing in the seasonal variability of sea surface salinity (SSS). Seasonal and interannual variations of SSS and sea surface temperature (SST) were analyzed in the south Pacific convergence zone (SPCZ) (Gouriou and Delcroix, 2002). Johnson et al. (2002) studied the relation between surface fresh water flux and salinity advection in the tropical Pacific, with the latter computed from salinity climatology and satellite-derived surface current (Bonjean and Legerloef, 2001). The improved spatial and temporal resolution in the derived data sets will help us better understand the atmospheric hydrological cycle at the ocean surface and the role of fresh water flux in the salinity perturbations.

2. DATA AND METHODOLOGY

The computation of Θ requires the measurements of vertical profiles of wind vectors and humidity. They have come from rawinsonde measurements, which are extremely sparse over ocean. Liu (1993) proposed a method to estimate Θ , using surface wind vector (\mathbf{u}_s) and W , measured by space-based scatterometer and radiometers. The physical rationale and methodology is described in Liu and Tang (2004). To simplify the method and reduce errors, a relation between Θ and \mathbf{u}_s W was derived. A data set of Θ computed from rawinsonde measurements at available ocean stations and NCEP reanalysis for 2001 was formed and they are related to \mathbf{u}_s W computed from collocated \mathbf{u}_s from QuikSCAT and W from Special Sensor Microwaver/Imager (SSM/I) through nonparametric regression (Härdle, 1990). Using this relation, different sets of high-resolution Θ are computed from various combinations of space-based \mathbf{u}_s and W . E is estimated from space-based radiometer based on a method by Liu et al. (1994).

The surface wind vectors used in this study include measurements from NASA's scatterometer – QuikSCAT (Liu 2002) and those produced by Atlas et al. (1996) by combining wind speed measured by SSM/I and other available

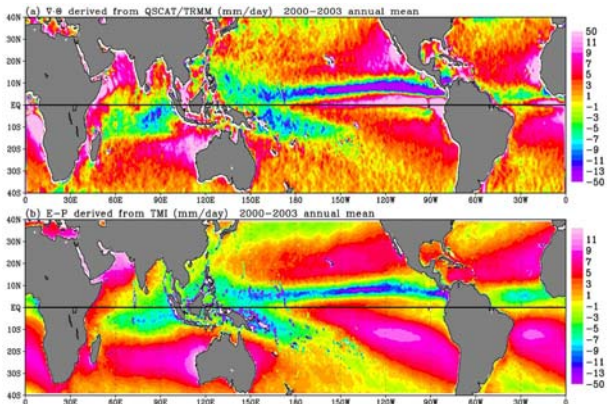


Fig. 1 Annual mean of (a) $\nabla \cdot \Theta$ and (b) $E - P$ in mm/day, averaged from 2000–2003, derived from QuikSCAT and TMI.

information on wind direction. The QuikSCAT wind starts from July 1999 to present with a spatial resolution of 25 km and twice daily sampling. SSM/I wind vectors cover the period from July 1987 to June 2003 and were interpolated to daily data at $1^\circ \times 1^\circ$ resolution. W and wind speed used to estimate E are from Tropical Rain Measuring Mission Microwave Imager (TMI) and SSM/I derived by Wentz (1997), with $0.25^\circ \times 0.25^\circ$ and twice daily resolution. SST is retrieved from TMI with the same resolution and NOAA OISST (Optimum Interpolation sea surface temperature) with $1^\circ \times 1^\circ$ resolution to derive the longer time series of E. P is from the TMI gridded orbital data mapped to $0.5^\circ \times 0.5^\circ$ grid, and from SSM/I from 1987. In the following sections, annual cycle was calculated using QuikSCAT and TMI, and interannual anomalies are based on SSM/I and OISST. Surface salinity from in situ measurements over the tropical Pacific was compiled by Delcroix et al. (1998) from 1969 to 2001. Since 1996, salinity is also collected from the equatorial mooring (McPhaden et al. 1998).

3. ANNUAL MEAN AND SEASONAL VARIABILITY

At the seasonal time scale, $\nabla \cdot \Theta$ should balance E-P because the first term in Eq. (1) is negligible. Fig. 1 shows that

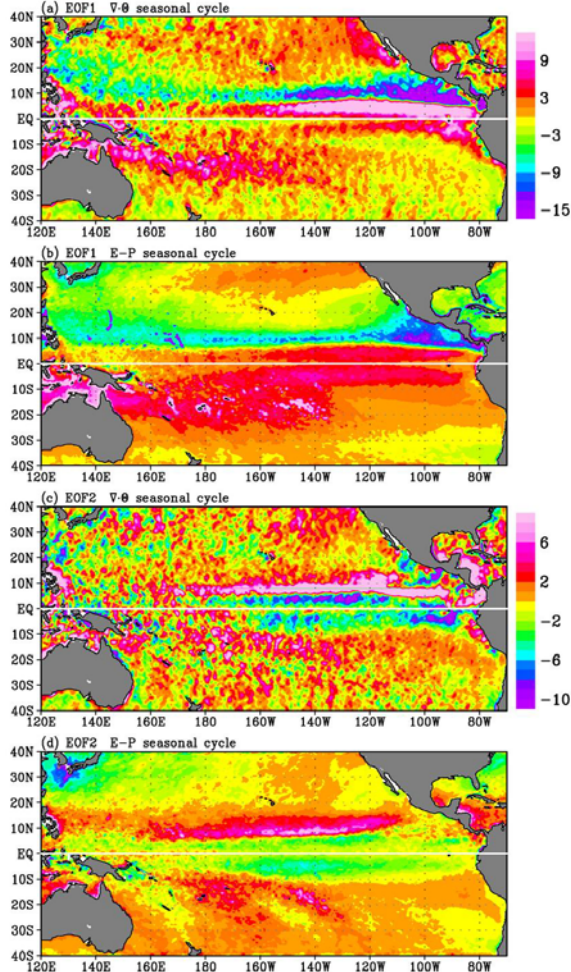


Fig. 2 The first EOF of $\nabla \cdot \Theta$ (a), E-P (b), the second EOF of $\nabla \cdot \Theta$ (c), and E-P (d) seasonal cycle. Annual mean is removed from the data.

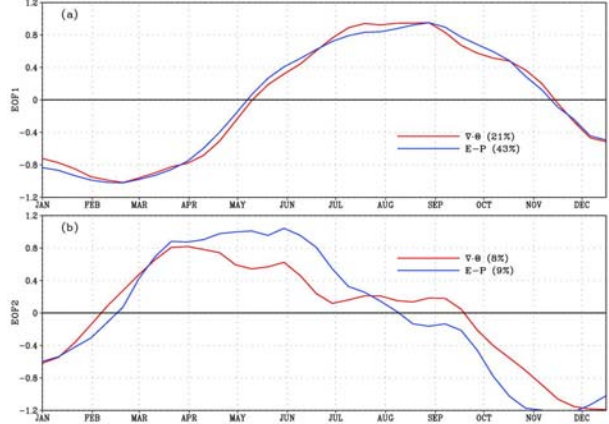


Fig. 3 Time series of the first EOF (a) and second EOF (b) of $\nabla \cdot \Theta$ and E-P seasonal cycle. Annual mean is removed from the data.

the annual mean of $\nabla \cdot \Theta$ bears similar large-scale features as that of E-P, over the ocean between 40°S - 40°N where TMI data are available. Both clearly demonstrate convergence/precipitation associated with the deep convection of the ITCZ across Pacific and Atlantic, the western Pacific warm pool, the SPCZ, the equatorial Indian Ocean, and, to a lesser intensity, the extension of Kuroshio and Gulf Stream. High evaporation in the subtropics may supply the moisture which is transported to fuel the deep convection. There are notable discrepancies between $\nabla \cdot \Theta$ and E-P. In the eastern Pacific, convergence of Θ over ITCZ and divergence of Θ near the equator are much stronger than E-P, whereas the convergence of Θ in the western Pacific warm pool is weaker than E-P. At finer scales, $\nabla \cdot \Theta$ and E-P do not agree very well in South China Sea, the eastern part of Bay of Bengal, and near the east coast of Africa. The extensions of Kuroshio and Gulf Stream are not as well defined in $\nabla \cdot \Theta$ as in E-P.

To examine the similarities and differences of their temporal variability, the EOF (empirical orthogonal function) spatial patterns and time series of $\nabla \cdot \Theta$ and E-P, with annual mean removed, are compared in Fig. 2 and Fig. 3. The first EOF (representing 21% and 43% of the total variances for $\nabla \cdot \Theta$ and E-P) structures are characterized by meridional asymmetry, which represents the latitudinal shift of seasonal cycle. Maximum precipitation and $\nabla \cdot \Theta$ reach their farthest location north of the equator during late boreal summer and are the closest to the equator during the end of winter. The second EOFs (accounting for 8% and 9% of the total variances

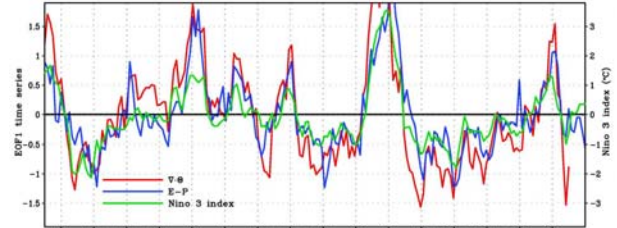


Fig. 4 Time series of the first EOF of $\nabla \cdot \Theta$ and E-P interannual anomalies, derived from SSM/I and OISST, compared with Nino3 index. Interannual anomalies are computed by removing the annual cycle from monthly mean.

for $\nabla \cdot \Theta$ and E-P) show double ITCZ over the eastern Pacific, strongest during the boreal spring (Liu and Xie, 2002).

4. INTERANNUAL VARIABILITY

To examine the interannual variations of the hydrological cycle, the computation of $\nabla \cdot \Theta$ and E-P is extended back to July 1987 by applying SSM/I and OISST data. After the annual cycle is removed, EOF analysis was performed with the anomalies. The time series of the first EOF of both $\nabla \cdot \Theta$ and E-P (representing 7% of the total variance) correlated well with the Niño3 index, indicating that ENSO signal is the leading mode in the interannual time scale (Fig. 4). They capture all the warm and cold episodes of ENSO.

The spatial pattern of the first EOF displays a coherent structure with ENSO warm events: the climatological deep convection in the tropical western Pacific warm pool migrates eastward and the northern hemisphere ITCZ shifts southward, resulting in enhanced convection in the central/eastern equatorial Pacific and suppressed convection in the equatorial western Pacific, the SPCZ, and north of the ITCZ (Fig. 5). EOF analysis of E and P separately indicates that suppressed fresh water flux to the ocean in the SPCZ during ENSO warm events are contributed by both increased evaporation due to stronger wind and reduced precipitation (figure not shown). The increase of fresh water flux to the ocean in the equatorial central Pacific is mainly contributed by enhanced convection, whereas contribution from suppressed evaporation due to weakened easterly trade wind is secondary. This may also attribute to low wind speed and small standard deviation of evaporation in this region.

The major differences between $\nabla \cdot \Theta$ and E-P are that both positive and negative anomalies of $\nabla \cdot \Theta$ are stronger than those of E-P in the equatorial eastern Pacific, and weaker in the equatorial western/central Pacific and the SPCZ.

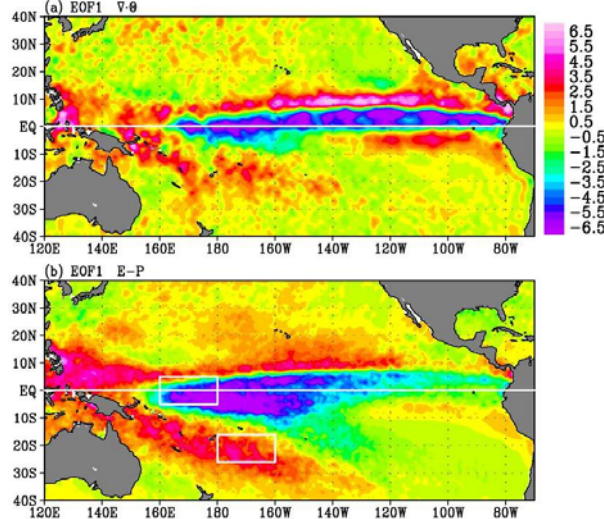


Fig. 5 The first EOF spatial pattern of (a) $\nabla \cdot \Theta$ and (b) E-P interannual anomalies.

5. SALINITY VARIATIONS

Due to limited salinity and ocean current observation, it is difficult to calculate salinity advection in the ocean. But we are able to use available salinity data in the tropical Pacific to study the relation with the fresh water flux. Fig. 5 highlights

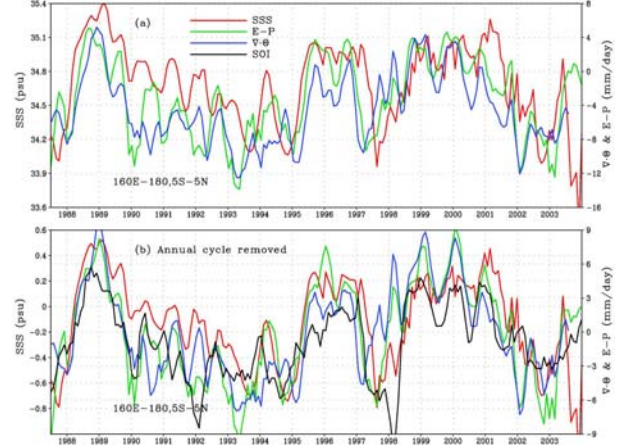


Fig. 6 Time series of area average of $\nabla \cdot \Theta$ and E-P between 160°E - 180° , 5°S - 5°N (the upper box in Fig. 5), with annual cycle (a) and annual cycle removed (b). SSS and SOI are superimposed.

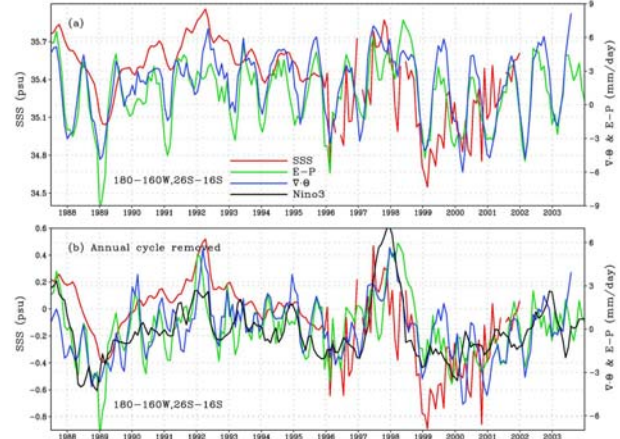


Fig. 7 Same as Fig. 6, except for 180° - 160°W and 16°S - 26°S (the lower box in Fig. 5). SSS and Nino3 index are superimposed.

two areas with enhanced (160°E - 180° , 5°S - 5°N) and suppressed (180° - 160°W , 26°S - 16°S) fresh water flux to the ocean, where sufficient salinity data were collected from repeated ship tracks.

Time series of the two area averages of $\nabla \cdot \Theta$, E-P, and SSS are compared in Fig. 6 and Fig. 7. $\nabla \cdot \Theta$ and E-P agree well in both seasonal and interannual time scales. SSS tends to increase during La Niña years and decrease during El Niño years in the equatorial central Pacific, which is positively correlated with the Southern Oscillation Index (SOI). This is consistent with less fresh water flux to the ocean during La Niña and more fresh water flux during El Niño. There is a clear freshening trend from the beginning of 1989 to the end of 1995, when the equatorial central Pacific experienced persistent warming, and consequently larger than normal precipitation. On the contrary, the surface water becomes saltier from the end of 1997 to the beginning of 2001, when the equatorial central Pacific shifts from abnormal warming to cooling. It is noted that E-P sharply decreases from the beginning of 1989 to the beginning of 1990 whereas salinity

gradually decreases. The annual variation of SSS is considerably smaller than its interannual variability. We need to further study whether this is true or simply because of inadequate data sampling to resolve high frequency variability.

In the SPCZ, the interannual anomalies of SSS, E-P, and $\nabla \cdot \Theta$ is positively correlated with the Niño3 index and is out of phase with that in the equatorial central Pacific (Fig. 6 and Fig. 7), as indicated in the first EOF (Fig. 5). E-P and $\nabla \cdot \Theta$ have well defined annual cycle with the strongest fresh water flux to the ocean in austral summer and the weakest in winter.

6. SUMMARY

Major components of hydrological cycle, $\nabla \cdot \Theta$ and E-P, are estimated over the ocean by applying high resolution space-based observations from scatterometers and microwave radiometers. Rawinsonde station data combined with NCEP reanalysis were used to derive the relation between Θ and collocated $\mathbf{u}_s \cdot \mathbf{W}$ measured by QuikSCAT and SSM/I. A tentative balance between $\nabla \cdot \Theta$ and E-P, their seasonal cycle and interannual variability, and their relation with SSS in the tropical Pacific were studied in this paper.

The annual mean of the estimated $\nabla \cdot \Theta$ and E-P have similar large scale structure: both capture major features over the tropical and subtropical oceans: (1) deep convection in the Pacific and Atlantic ITCZ, the western Pacific warm pool, the SPCZ, the equatorial Indian Ocean, and the extensions of Kuroshio and Gulf Stream, and (2) high E in the subtropics outside the deep convective regions. The seasonal variability of $\nabla \cdot \Theta$ and E-P is characterized by the latitudinal shift of moisture convergence and deep convection of the ITCZ, with a double ITCZ in the boreal spring.

The leading mode of the interannual fluctuation of $\nabla \cdot \Theta$ and E-P is ENSO related. The spatial pattern displays a coherent structure with ENSO events; deep convection in the western Pacific warm pool shifts eastward to the equatorial central Pacific, resulting in low salinity, and the Pacific ITCZ moves southward. The time series of the leading EOF mode positively correlated with SOI in the equatorial central Pacific. In the SPCZ, the interannual anomalies tend to be out of phase with the equatorial central pacific, with stronger evaporation, reduced convection, and high salinity during the warm events. This scenario is consistent with the study of Gouriou and Delcroix (2002).

Because of the sparse salinity observational data, the hydrological budget for the ocean is limited in this study. With the advance in ocean general circulation model (OGCM), we will further our understanding of how the fresh water flux and salinity fluctuate over a wide spectrum of time scales in the global ocean and the closure of hydrological cycle of the coupled ocean-atmosphere system. The algorithms to estimate E and Θ will be improved to help us better understand the global hydrological budget.

ACKNOWLEDGMENT This study was performed at the Jet Propulsion Laboratory, California Institute of Technology, under contract with the National Aeronautics and Space Administration (NASA). It was supported jointly by the Physical Oceanography, the Ocean Vector Wind, the Earth System Science, and the TRMM programs of NASA.

REFERENCES

- Atlas, R., R. Hoffman, S. Bloom, J. Jusem, J. Ardizzone, 1996: A multi-year global surface wind velocity data set using SSM/I wind observations. *Bull. Amer. Meteor. Soc.*, 77, 869-882.
- Bonjean, f., and G.S.E. Lagerloef, 2001: diagnostic model and analysis of he surface currents in the tropical Pacific ocean. *J. Phys. Oceanogr.*, 32, 2938-2954.
- Delcroix, T., L. Goudeau, and C. Henin, 1998: Sea surface salinity changes along the Fiji-Japan shipping track during the 1996 La Nina and 1997 El Nino period. *Geophys. Res. Lett.*, 25, 3169-3172.
- Delcroix, T., and C. Henin, 1991: Seasonal and interannual variations of sea surface salinity the the tropical Pacific Ocean. *J. Geophys. Res.*, 96, 22135-22150.
- Härdle, W., 1990: Applied Nonparametric Regression. Cambridge University Press, 333 pp.
- Gouriou, Y., and T. Delcroix, 2002: Seasonal and ENSO variations of sea surface salinity and temperature in the south Pacific convergence zone during 1976-2000. *J. Geophys. Res.*, 107(C12), doi:10.1029/2001JC000830.
- Johnson, E.S., G.S.E. Lagerloef, J.T. Gunn, and F. Bonjean, 2002: Surface salinity advection in the tropical oceans compared with atmospheric freshwater forcing: a trail balance. *J. Geophys. Res.*, 107(C12), 8014, doi:10.1029/2001JC001122.
- Liu, W. T., 1993: Ocean Surface Evaporation. *Atlas of Satellite Observations Related to Global Change*, R.J. Gurney, J. Foster, and C. Parkinson (eds.), Cambridge University Press, Cambridge, 265-278.
- Liu, W.T., 2002: Progress in scatterometer application, *J. Oceanogr.*, 58, 121-136.
- Liu, W.T. and X. Xie, 2002: Double Intertropical Convergence Zoens – a new look using scatterometer. *Geophys. Res. Lett.*, 29(22), 2072, doi:10.1029/2002GL015431.
- Liu, W. T. and W. Tang, 2004: Moisture transport over ocean observed from space. *J. Geophys. Res.*, in press.
- Liu, W.T., A. Zheng, and J. Bishop, 1994: Evaporation and solar irradiance as regulators of the seasonal and interannual variabilities of sea surface temperature, *J. Geophys. Res.*, 99, 12623-12637.
- McPhaden, M. J., A. J. Busalacchi, R. Cheney, J. R. Donguy, K. S. Gage, D. Harlpern, M. Ji, P. Julian, G. Meyers, G. T. Mitchum, P. P. Niiler, J. Picaut, R. W. Reynolds, N. Smith, and K. Takeuchi, 1998: The Tropical Ocean-Global Atmosphere (TOGA) observing system: A decade of progress, *J. Geophys. Res.*, 103, 14,169-14,240.
- Wentz, F.J., 1997: A well-calibrated ocean algorithm for Special Sensor Microwaver/Imager, *J. Geophys. Res.*, 102 (C4), 8703-8718.